Salvador Rubio, FJ.; Plazas Torres, AH.; Gimeno García, J.; Carreres Talens, M. (2014). Complete modelling of a piezo actuator last-generation injector for diesel injection systems. International Journal of Engine Research. 15(1):3-19. doi:10.1177/1468087412455373.

Complete modelling of a piezo actuator last generation injector for diesel injection systems

F. J. Salvador, A. H Plazas, J. Gimeno and M. Carreres

CMT-Motores Térmicos, Universitat Politècnica de València, Spain

Corresponding author:

Francisco Javier Salvador, CMT-Motores Térmicos, Universitat Politècnica de València, Camino de Vera s/n, E-46022, Spain.

Email: fsalvado@mot.upv.es

Abstract

An experimental and computational study of the increasingly used third generation common rail injection system with piezo actuator has been carried out. A complete characterization of the different elements of the system, both geometrically and hydraulically, has been performed in order to describe its behavior. The information obtained through the characterization has been used to create a one-dimensional model that has been implemented in the commercial software AMESim and extensively validated against experimental data. The results of the validation demonstrate the model ability to predict the injection rate of the injector with high level of accuracy, therefore constituting a powerful tool in order to carry out further studies of this type of injection systems.

Keywords

Injector, modeling, Diesel, piezo

Introduction

Injection systems have a strong influence on the behavior of the injection rate and thus in phenomena such as spray atomization, combustion and emissions[1,2,3,4]. Bosch

common rail injectors have become the solution adopted by most manufacturers. In the last decade, solenoid operated injectors became the standard for most diesel engines [5,6,7,8]. However, piezoelectric operated injectors are increasingly being used by the manufacturers due to their quicker dynamics, which gives more flexibility in terms of injection strategies such as multiple injections[89,10]. Their faster dynamic response improves the stability of the pilot injections enhancing the reliability of the system. These facts suggest that the usage of piezoelectric injectors will increase in the near future. Therefore, it is important to develop tools that make it possible to predict the behavior of this kind of system in order to optimize their performance and solve any problem that could rise. In previous systems such as the solenoid injectors, one-dimensional modeling proved to be one of these tools[56,7,8]. Hence, a one-dimensional model of a Bosch piezoelectric injector is proposed in this study and implemented via the commercial software AMESim[11]. Once the model is introduced, it is validated against experimental data in order to demonstrate its performance and capabilities.

The present article adopts the following structure:

In the “How it works” section, an explanation of the working principle of piezoelectric injectors is given, describing their internal elements and how they relate to each other in order to command the injector hydraulically. Then, in the “Experimental facilities” section, the experimental tools utilized for the characterization of each of the inner components of the injector are described, based on two kinds of characterization: the

dimensional characterization and the hydraulic characterization of the restrictions. In the "Model description" section, the different parts of the proposed model are depicted (injector holder, control valve, nozzle and piezoelectric valve) and finally merged. At last, in the "Model validation" section, a comparison between the injection rate obtained by the model and the experimental results for different values of injection pressure and energizing times is performed.

How it works

Figure 1 shows the internal components of the injector: piezoelectric valve (which consists of a piezoelectric actuator, a hydraulic amplifier and a control valve), injector holder (high pressure fitting, filter, fuel return to pump, injector body) and nozzle.

The inner components of the piezoelectric valve are shown in detail in Figure 2. Unlike the typical solenoid injector, it has three active orifices (an outlet orifice and two inlet orifices). The outlet orifice (OAZ) also works as an inlet orifice. On the other hand, the control volume is placed directly over the valve, which improves the dynamic response of the injector and facilitates the introduction of multiple injections (up to eight consecutive injections). The maximum injection pressure that can be achieved by these injectors is 2000 bar.

A scheme of the injector working principle is depicted in Figure 3. When the piezoelectric actuator is not activated (Figure 3(a)), the upper seat of the control valve

(valve seat 1) is closed due to the preload force of the spring and the pressure exerted on the lower part of the valve bolt. As a consequence, the pressure in the control volume and the rest of the system is equal to the rail pressure. Since the area in the upper part of the needle is higher than the one in the lower part, the force on the upper part is greater, attaching the needle to its seat and thus resulting in no injection.

When the actuator is activated (Figure 3(b)) it expands, displacing the amplifier piston, which compresses the fuel located between the lower part of the amplifier piston and the upper part of the command piston. This fact amplifies the displacement of the command piston, opening the upper seat of the control valve and closing the lower one (valve seat 1 open and valve seat 2 closed). This amplification guarantees that the displacement of the command piston will always be enough to keep the lower seat of the control valve (valve seat 2) closed when the piezoelectric actuator is deformed, keeping the bypass orifice (OB) inactive.

Once the valve seat 1 opens, the pressure downstream of the outlet orifice is reduced until it reaches the backpressure value (1 MPa). Hence, the fuel in the control volume stops pressing the upper part of the needle and it flows towards the fuel return through the outlet orifice (OAZ) and the valve seat 1. The needle moves from its seat as the force exerted by the fuel surrounding the lower part of the needle is higher than the force on the upper part of it, resulting in the injection phenomenon.

Unlike the typical solenoid injectors, the only fuel that goes to the return is the one used for control tasks inside the injector, as there are no internal leakages. This means that the fuel only flows towards the fuel return when the injection is happening.

When the actuator is deactivated (Figure 3(c)), it returns to its initial length thanks to the tube spring. The valve seat 1 closes due to the valve spring preload, and the pressure on the upper part of the command piston is recovered as the fuel enters through the inlet orifice (OZ) and the outlet orifice (OAZ), because when the valve seat 2 opens it connects the inlet of the OZ orifice to the outlet of the OAZ orifice through OB orifice. This turns the OAZ orifice into a second inlet orifice. Finally, the needle is pushed towards its seat and thus ending the injection process.

Experimental facilities

The injection system used throughout this study is a conventional Common Rail Fuel Injection system[12,13], which makes it possible to reach high and relatively constant pressure values (up to 180 MPa). The injector where the nozzles were mounted is a third generation piezoelectric Bosch injector. Six-orifice sac nozzles were used for the study.

The fluid used for the experiments was Repsol CEC RF-06-99. Some of the characteristics of this fluid are depicted in Table 1.

The experimental tools used for the dimensional and hydraulic characterization of the injection system are the following ones:

1. Silicone molds and scanning electron microscope (SEM).
2. Hydraulic characterization test rigs.
3. Injection rate test rig.

Silicone moulds and scanning electron microscope (SEM)

In order to determine the nozzle's exact internal geometry a methodology described by Macián et al. is used[14]. The methodology is based on the use of a special type of silicone in order to obtain internal molds of the different parts of the injector. Once the molds have been obtained, pictures of them are taken with an optical microscope or a scanning electron microscope (SEM), depending on the size of the mold. Then, the pictures are processed with the help of computer aided design (CAD) software. Figure 4 depicts the process that corresponds to the use of an optical microscope. Obtaining the pictures with a scanning electron microscope is more complex since the samples need to be electrical conductors in order to evacuate the high energy of the electron beam used in the visualization. Therefore, the samples require a metal coating before they are ready to

be visualized. This coating must be thin enough so that the geometry is not modified. Figure 5 shows the process in this case, applying a gold coating to the samples.

The obtaining of the geometrical parameters of the nozzle orifices can be seen in Figure 6. The figure shows that these orifices are convergent, a fact that is important for the hydraulic characterization as it means that the orifices are not prone to cavitate[1516].

Hydraulic characterization test rigs

The hydraulic characterization is performed in order to evaluate the permeability of the internal calibrated orifices. The permeability, together with the geometrical information of the orifices obtained previously, makes it possible to determine the discharge coefficient of an orifice as a function of the pressure drop (Reynolds number).

The rigs are used to characterize either the nozzle orifices or the control volume orifices (OZ, OAZ and OB). In the first case (Figure 7), the nozzle is mounted in an empty nozzle holder where the needle has been removed in order to avoid any friction loss different from the one due to the orifices themselves. The injection pressure and the backpressure are controlled by a standard common rail injection system and a valve, respectively. For a given pressure, it is possible to measure the mass flow rate when the flow becomes steady. The curve on the left in Figure 8 shows the results of the hydraulic characterization of the nozzle. In the curve, the mass flow rate is plotted against the square root of the pressure drop for two injection pressures (10 and 20 MPa)

and several values of backpressure, showing that the mass flow rate increases linearly with the square root of the pressure drop as it is expected in convergent orifices, where cavitation is avoided[15,16,17].

At this point, the discharge coefficient can be obtained by combining the mass conservation equation and Bernoulli's equation. The former one leads to:

$$\dot{m} = C_d \cdot A_0 \cdot \rho_f \cdot u_B \tag{1}$$

The term u_B is the Bernoulli's theoretical velocity, which is given by the expression:

$$u_B = \sqrt{\frac{2 \cdot \left(P_{inj} - P_b \right)}{\rho_f}} \tag{2}$$

Combining equations (1) and (2), the discharge coefficient can be obtained as it was stated:

$$C_d = \frac{\dot{m}_f}{A_0 \cdot \sqrt{2 \cdot \rho_f \cdot \left(P_{inj} - P_b \right)}} \tag{3}$$

The curve on the right in Figure 8 displays the evolution of the discharge coefficient with the theoretical Reynolds number, also known as flow number. The Reynolds number is defined as:

$$\mathrm{Re} = \frac{D_0 \cdot u_0}{\nu_f} \tag{4}$$

The Reynolds number can be considered as a theoretical Reynolds number (flow number, λ) if the Bernoulli's theoretical velocity is considered instead of the actual velocity:

$$\lambda = \frac{D_0}{\nu_f} \cdot \sqrt{\frac{2 \cdot (P_i - P_b)}{\rho_f}} \tag{5}$$

The figure shows a continuous increase of the discharge coefficient with the flow number, until it reaches an asymptotic maximum value (C_{dmax}). This value and the critical flow number (defined as the value of the flow number which corresponds to a discharge coefficient value of 95% of C_{dmax}) have been depicted in the curve. These parameters are used in the 1D model to define the hydraulic behavior of the orifices and are heavily influenced by the orifice geometry[1,2,3,7,8,15,16,17,18,19].

On the other hand, in the case of the control orifices, different test rigs are used for the hydraulic characterization. Their working principle consists in isolating the calibrated orifice to be tested so that the fuel only flows through it. Figure 9 shows the test rig corresponding to the OZ orifice as an example. The pressure both upstream and downstream the orifice is controlled in a similar way as it is done for the nozzle orifices: the fluid is supplied by a high pressure pump and it passes through the calibrated orifice, which is connected to a volume where the backpressure is also controlled. The variation of the mass flow rate against the square root of the pressure drop for the control orifices is depicted in Figure 10. Again, two values of injection pressure (10 and

20 MPa) have been considered, varying the backpressure from these values to the atmospheric pressure. It can be seen that, for low values of the pressure drop, the mass flow rate increases linearly with the square root of the pressure drop. However, the mass flow rate remains constant from a certain value of the pressure drop. This behavior was expected due to the fact that the control orifices are cylindrical and thus prone to cavitate[15,16,19]. The values of the pressure drop that lead to the choking of the mass flow rate are the critical cavitation conditions and are strongly related to the inception of cavitation[20]. Several parameters have been defined in the literature to describe the tendency of an orifice to cavitate. The cavitation number introduced by Soteriou et al. has been considered in this study[21]:

$$CN = \frac{P_i - P_b}{P_b - P_v} \tag{6}$$

The vapor pressure is usually neglected due to its small value when compared to both the injection pressure and the backpressure. The critical cavitation number (CN_{crit}) corresponds to the pressure drop for which cavitation starts and it is detected through the stabilization of the mass flow rate. When the orifices do not cavitate, the discharge coefficient increases with the Reynolds number in the same way it was described for non-cavitating orifices (right curve in Figure 8). However, under cavitating conditions ($CN > CN_{crit}$), the discharge coefficient stops increasing depending on the Reynolds number and varies with the cavitation number as described by the following expression:

$$C_d = C_c \cdot \sqrt{1 + \frac{1}{CN}} \tag{7}$$

where C_c is the contraction coefficient in the orifice that occurs due to cavitation and is obtained by particularizing the equations for the critical cavitation conditions (CN_{crit}) for which the discharge coefficient is known. Table 2 shows the parameters obtained through the characterization of the control orifices, which will be used in the 1D model. The diameters have been obtained following the procedure described in the "Experimental facilities" section as shown in Figure 11.

Injection rate meter

Tests of injection rate were carried out with an Injection Rate Discharge Curve Indicator (IRDCI) commercial system. This device makes it possible to display and record the data that describe the chronological sequence of an individual fuel injection event. The measuring principle used is the Bosch method[12], which consists of a fuel injector that injects into a fuel-filled measuring tube. The fuel discharge produces a pressure increase inside the tube which is proportional to the increase in fuel mass. The rate of this pressure increase corresponds to the injection rate. A pressure sensor detects this pressure increase and an acquisition and display system processes the recorded data for further use.

Model description

AMESim, a commercial software package for multi-domain 1D system simulation, has been used to develop the model in the present study[11]. AMESim offers libraries for the different physical domains (mechanic, hydraulic, electrical, etc.) with a wide range of components that can be connected to simulate the physical properties of a system. The proposed model for the piezoelectric injector can be divided into four parts: injector holder, control valve, nozzle and piezoelectric valve.

The stiffness rate values of the different springs of the injector have been calculated applying the theoretical equation used by Bosch[22]:

$$K_{spring} = \frac{G_{steel} \cdot d_{spire}^4}{8 \cdot N_{spires} \cdot D_{spring}^3} \tag{8}$$

It is important to note that, due to the high pressures achieved in common rail injectors, the elastic deformations of the mechanical elements may achieve high values, reaching even the same order of magnitude of their displacements. Thus, the deformations need to be taken into account. The method followed by Payri et al.[6] and Desantes et al.[23] is used in the present work. It simulates the deformations of each mechanical element by means of a spring with an equivalent stiffness rate defined by the following equation:

$$K_{equivalent} = \frac{1}{\frac{1}{E_{steel}} \cdot \sum \frac{L_i}{A_i}} \tag{9}$$

Model of the injector holder

A sketch of the AMESim injector holder model can be seen in Figure 12(a), whereas Figure 12(b) offers a detail of the inner ducts of the injector holder. In the model, a constant pressure source simulates the pressure signal generated by the high pressure pump. This pressure source feeds a 24 cm^3 volume which represents the rail. This volume is connected to the injector holder through the high pressure line HPL1. The restriction HPF simulates the high pressure fitting filter, after which the line L1 feeds the control valve. On the other hand, the injector holder has two other lines (L4 and L5) whose function is to return the fuel that comes from the control valve to the low pressure circuit of the common rail system. The fuel return pressure is 10 bar. The values of the main parameters used to define these elements are collected in Table 3. Figure 13 shows the dimensional characterization of the lines of the injector holder.

Model of the control valve

Figure 14 gives a detail of the model (Figure 14(a)) and the basic elements of the control valve (Figure 14(b)). The line L1 feeds the volume V1 through the line L2. In

this volume, the flow is divided in two directions: through line L3 and through the OZ orifice. The flow coming from line L3 feeds the nozzle through the volume NV1. This volume is connected to the volume V3 by means of the variable section orifice OV2, which simulates the lower seat of the control valve. On the other hand, the OZ orifice is connected to the volume V2, which is linked to the volume V3 through the OAZ orifice.

The element OV2 is mechanically related to the element OV1 thanks to the mechanical elements VBM and VBD. The element VBM simulates the valve bolt mass. The area of the variable orifices OV1 and OV2 is determined by the displacement of the valve bolt, which is affected by the high pressure forces exerted by the fluid and the mechanical forces transmitted by the hydraulic amplifier and the valve spring VS. This deformation leads to an increase in the area of those orifices. Therefore, the element VBD simulates the valve bolt deformation. Figure 15 shows the valve bolt dimensions obtained by using the technique explained in the “Experimental facilities” section and its equivalent stiffness rate.

The variable orifice OV1 connects the volume V3 to the volume V4, which is connected to the hydraulic amplifier in turn. This variable orifice is simulated with a ball seat valve. Since the upper seat of the valve does not have this geometry, it is necessary to calculate the equivalent diameter of the ball. The dimensional characterization makes it possible to determine the closing point of the upper seat. The different diameters

obtained in the dimensional characterization of the upper and lower control valve seats can be seen in Figure 16. The valve bolt diameter at the upper seat contact point (d_a in the figure) can be related to the ball diameter through the cosine of the semiangle (α), from where the value of the ball diameter is calculated.

The variable orifice OV2 is simulated with a plain seat valve. The diameter of this valve (d_s in Figure 16) is the value of the bypass orifice diameter.

The dimensions of the ducts, volumes and inner components of the control valve are obtained using the technique described in the "Experimental facilities" section. The dimensional characterization of the orifices can be seen in Figure 17, whereas Figure 18 shows the volumes obtained by overlapping the pictures of the valve bolt and the valve holder.

The values of the main parameters used for the control valve elements are collected in Table 4.

Model of the nozzle

Figure 19 shows the different basic elements of the nozzle and its corresponding model in AMESim. The nozzle model is linked to the control valve model through a hydraulic connection (the piston NP1 and the internal leakages NFFI with the volume V2 and the

volume NV1 with the line L3). The control volume V2 is located in the upper part of the nozzle body. This volume actuates directly on the piston NP1. Additionally, the volume NV1 is connected to the element NFFI, which simulates the friction and internal leakages between the needle and the control volume V2, and with the line NL1 that feeds the volume NV2. This volume is in charge of distributing the pressure uniformly where the needle changes its section (NP2).

The line NL2 is located downstream of the volume NV2 and is connected to the volume NV3 and the piston NP3. The elements NP2, NP3 and NL2 are determined by the geometry of the needle cross section. The cross section of the needle where the fuel travels through towards the volume NV3 is divided in three parts, as can be seen in the cross section depicted in Figure 19. Each section of the needle is simulated rather than simulating the area as a whole (NL2). The lines NL2 feed the volume NV3, which distributes the pressure over the piston NP3. The line NL3 is located downstream of the volume NV3 and feeds the volume NV4, which is located in the upper part of the nozzle seat OV3 and is connected to the piston NP4. The nozzle seat OV3 is simulated by a conical seat, whose configuration depends on the geometry of the nozzle (micro-sac in this study). The geometrical characterization of the volumes and inner sections of the nozzle seat is obtained by overlapping the silicon molds pictures and the needle pictures, as can be seen in Figure 20. On the other hand, due to the needle configuration, it would not be correct to assume its deformation to be uniform along its length. Hence,

the needle has been divided into three sections and the equivalent stiffness rate has been obtained for each of them using equation (9).

A summary of the main parameters used for the nozzle model are shown in Table 5.

Model of the piezoelectric valve

The configuration of the piezoelectric valve and the proposed model can be seen in Figure 21. The model is composed of an ideal source of voltage VS that is connected to the piezoelectric actuator. It produces an expansion of the piezoelectric actuator that compresses the tube spring TS and displaces the amplifier piston, which is simulated by the elements APM, APFFI and AP. The element APM simulates the inertia of the amplifier piston and the mechanical friction. The element APFFI simulates the internal leakages and the viscous friction between the hydraulic amplifier body and the amplifier piston. The internal leakages are connected to the fuel return line L4 of the injector holder model. Finally, the element AP recreates the pressure force that is exerted by the fuel in the volume V5.

The displacement of the amplifier piston tries to reduce the volume V5. This leads to a pressure increase and pushes the fluid to exert a force on the command piston VPM. This force is simulated by the element VP1. Since the area of the command piston is lower, the displacement of the piezoelectric actuator is amplified by a 1.5 factor. As it is

done for the amplifier piston, the elements VPFFI and VPM represent the internal leakages, the viscous friction, the mechanical friction and the inertia.

The element VPS simulates the valve piston spring, which is preloaded for maintaining that piston in contact with the valve bolt. The piston VP2 represents the pressure force exerted by the fluid on the lower part of the command piston, which is in contact with the volume V4. The fluid coming from the hydraulic connection with the control valve and the internal leakages of the command piston flows through the orifices AO located in the body of the hydraulic amplifier, which are connected to the fuel return line L4 together with the leakages of the amplifier piston.

As in the previous cases, the initial deformations of the springs, displacement of the elements, diameters, clearance between elements, etc. have been obtained thanks to the metrology of the elements. Figure 22 shows the geometrical characterization of the hydraulic amplifier body, obtained by using the technique described in the "Experimental facilities" section. As it was stated, the values of the stiffness rate of the springs have been calculated applying equation (8). However, there are two elements that require an experimental characterization: the tube spring TS and the piezoelectric actuator. The spring TS has a non conventional geometry and therefore the stiffness rate is obtained through experimental means. The force-deformation points obtained for the spring can be seen in Figure 23 together with a fitted function and its analytical

expression. The slope of this function is the stiffness rate of the spring. On the other hand, the most important parameter of a piezoelectric material is the relation among the applied voltage and the displacement of the material. Tests were carried out at different voltages for the piezoelectric actuator, as can be seen in Figure 24.

The main parameters used for the piezoelectric valve model are summarized in Table 6.

Model validation

A complete sketch of the model compiling the different parts described in the previous sections is shown in Figure 25.

Several experimental tests were carried out in order to validate this model, using the injection rate meter described in the "Experimental facilities" section. Three injection pressures were explored: 300, 800 and 1600 bar. For each of these pressures, four different energizing times were considered: 0.25, 0.5, 1 and 2 ms. The experimental results are compared to those obtained by the proposed model in Figure 26. This figure, together with the total mass injected comparison shown in Figure 27, highlights the ability of the model to predict the actual behavior of the injector with a considerable level of accuracy.

Conclusions

The present work describes a methodology to model a common rail diesel injection system and specifically a third generation (piezoelectric) Bosch injector. This methodology is based on a previous characterization of the injector, attending to two criteria:

- The geometry of the internal elements of the injector, which is characterized through the obtaining of silicon moulds of these elements and their subsequent visualization by using an optical microscope or a scanning electron microscope (SEM).
- The hydraulic behavior of the internal restrictions of the injector, which is determined by carrying out several tests through the usage of different test rigs implemented for this purpose.

Once the internal components of the injector have been characterized, a one-dimensional model has been implemented through the commercial software AMESim and validated afterwards for different starting conditions. The results of this validation highlight the ability of the model to accurately predict the behavior of the injector in terms of injection rate.

Funding

This work was supported by the Ministerio de Ciencia e Innovación in the frame of the project “Estudio teórico experimental sobre la influencia del tipo de combustible en los

procesos de atomización y evaporación del chorro Diesel (PROFUEL)" [grant number TRA 2011-26293]. This support is gratefully acknowledged by the authors.

References

1. Payri R, Molina S, Salvador FJ, et al. A study of the relation between nozzle geometry, internal flow and sprays characteristics in diesel fuel injection systems. *KSME International Journal* 2004, 18 (7): 1222-1235.

2. Bermúdez V, Payri R, Salvador FJ, et al. Study of the influence of nozzle seat type on injection rate and spray behavior. *Proceedings of the Institution of Mechanical Engineers Part D-Journal of Automobile Engineering* 2005, 219 (D5): 677-689.

3. Kent JC and Brown GM. Nozzle exit flow characteristics for square-edged and rounded inlet geometries. *Combust Sci Technol* 1983, 30: 121-132.

4. Payri R, Salvador FJ, Gimeno J et al. Effects of nozzle geometry on direct injection diesel engine combustion process. *Appl Therm Eng* 2009, 29 (10): 2051-2060.

5. Payri R, Climent H, Salvador FJ, et al. Diesel injection system modelling. Methodology and application for a first generation common rail system. *Proceedings of the Institution of Mechanical Engineers Part D-Journal of Automobile Engineering* 2004, 218 (D1): 81-91.

6. Payri R, Tormos B, Salvador FJ, et al. Using one-dimensional modelling codes to analyse the influence of diesel nozzle geometry on injection rate characteristics. *Int J Veh Des* 2005, 38 (1): 58-78.

7. Payri R, Salvador FJ, Martí-Aldaraví P, et al. Using one-dimensional modeling to analyse the influence of the use of biodiesels on the dynamic behavior of solenoid-operated injectors in common rail systems: detailed injection system model. *Energy Convers Manage* 2012, 54: 90-99.

8. Salvador FJ, Gimeno J, De la Morena DJ, et al. Using one-dimensional modeling to analyse the influence of the use of biodiesel son the dynamic behavior of solenoid-operated injectors in common rail systems: Results of the simulations and discussion. *Energy Convers Manage* 2012, 54: 122-132.

9. Payri R, Salvador FJ, Gimeno J, et al. Influence of injector technology on injection and combustion development – Part 1: Hydraulic characterization. *Appl Energy* 2011, 88 (4): 1068-1074.

10. Payri R, Salvador FJ, Gimeno J, et al. Influence of injector technology on injection and combustion development – Part 2: Combustion analysis. *Appl Energy* 2011, 88 (4): 1130-1139.

11. LMS Imagine. Lab AMESim v.8. User's manual, 2010.

12. Payri R, Salvador FJ, Gimeno J, et al. A new methodology for correcting the signal cumulative phenomenon on injection rate measurements. *Exp Tech* 2008, 32 (1): 46-49.

13. Flaig U, Polach W and Zieglet G. Common rail system (CR-System) for passenger car DI Diesel engines. Experiences with applications for series productions projects. SAE paper 1999-01-0191, 1999.

14. Macián V, Bermúdez V, Payri R, et al. New technique for the determination of the internal geometry of diesel nozzle with the use of the silicone methodology. *Exp Tech* 2003, 27 (2): 39-43.

15. Macián V, Payri R, Margot X, et al. A CFD Analysis of the Influence of Diesel Nozzle Geometry on the inception of Cavitation. *Atomization Sprays* 2003, 13: 579-604.

16. Payri F, Bermúdez V, Payri R, et al. The influence of cavitation on the internal flow and the spray characteristics in diesel injection nozzles. *Fuel* 2004, 83: 419-431.

17. Ohrn TR, Senser DW and Lefèbvre AH. Geometrical effects on discharge coefficients for plain-orifice atomizers. *Atomization Sprays* 1991, 1 (2): 137-153.

18. Lichtarowicz A, Duggins RK and Markland E. Discharge coefficients for incompressible non-cavitating flow through long orifices. *Journal of Mechanical Engineering Science* 1965, 7 (2).

19. Salvador FJ, Romero JV, Roselló MD, et al. Validation of a code for modeling cavitation phenomena in Diesel injector nozzles. *Math Comput Modell* 2010, 52 (7-8): 1123-1132.

20. Payri R, Salvador FJ, Gimeno J, et al. Study of cavitation phenomena based on a technique for visualizing bubbles in a liquid pressurized chamber. *Int J Heat Fluid Flow* 2009, 30: 768-777.

21. Soteriou C, Andrews R and Smith M. Further studies of cavitation and atomization in Diesel injection. SAE paper 1999-01-1486, 1999.

22. Adler U. *Automotive Handbook*. 3rd ed. Stuttgart: Robert Bosch GmbH, 1996.

23. Desantes JM, Arrègle J and Rodríguez PJ. Computational model for simulation of diesel injection systems. SAE Paper 1999-01-0915, 1999.

Appendix 1: notation

A_i: area of the fraction *i* of an element

A_o: geometrical area

C_c: contraction coefficient

C_d: discharge coefficient

CN: cavitation number

C_v: velocity coefficient

d_{spire}: spring spire diameter

D_o: diameter at the orifice outlet

D_{spring}: spring diameter

E_{steel}: steel Young's modulus

G_{steel}: steel shear modulus

$K_{equivalent}$: equivalent stiffness rate

K_{spring}: spring stiffness rate

L_i: length of the fraction *i* of an element

$\dot{m}_f$: mass flow

N_{spires}: spring number of spires

P_{back}: discharge back pressure

P_{inj}: injection pressure

P_v: vapor pressure

Re: Reynolds number

u_o: actual velocity at the orifice outlet

u_B: theoretical velocity, $u_B = \sqrt{\frac{2\Delta P}{\rho_f}}$

ΔP: pressure drop, $\Delta P = P_{inj} - P_{back}$

λ: flow number

ρ_f: fuel density

v_f: fuel kinematic viscosity

Subscripts

crit: cavitation critical conditions

Appendix 2: List of tables

Appendix 3: List of figures

Appendix 3: List of figures

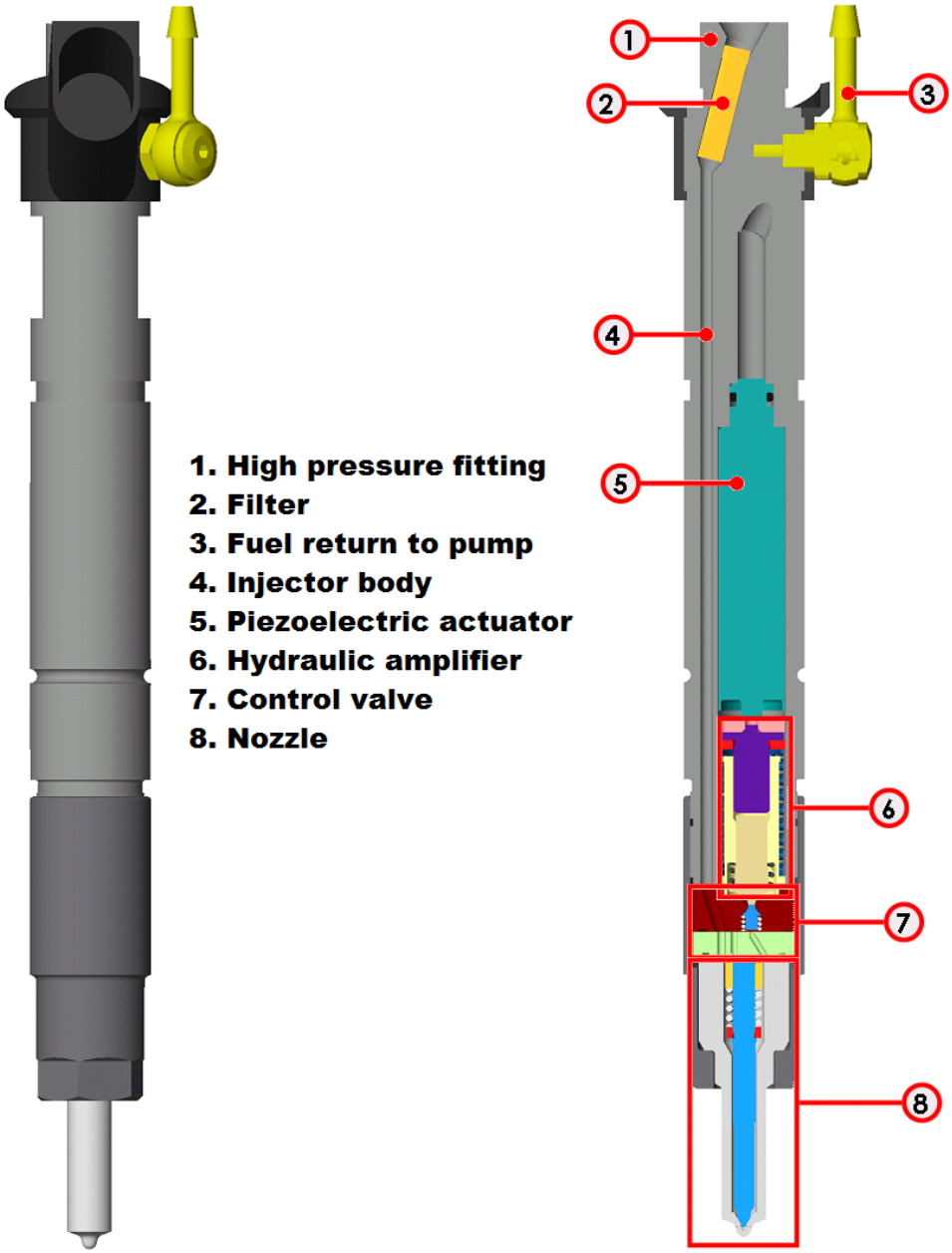

Figure 1. Internal components of a piezoelectric injector.

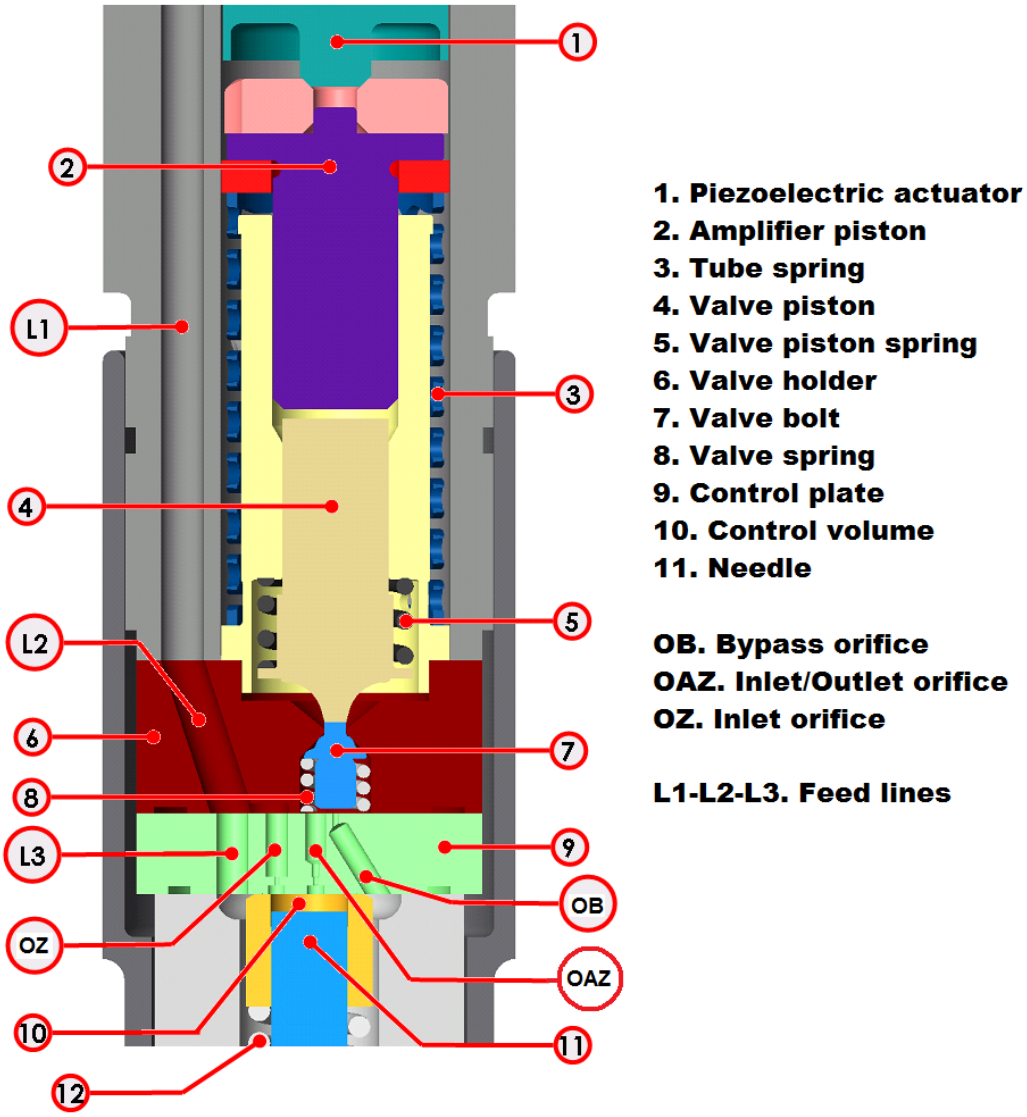

Figure 2. Piezoelectric valve.

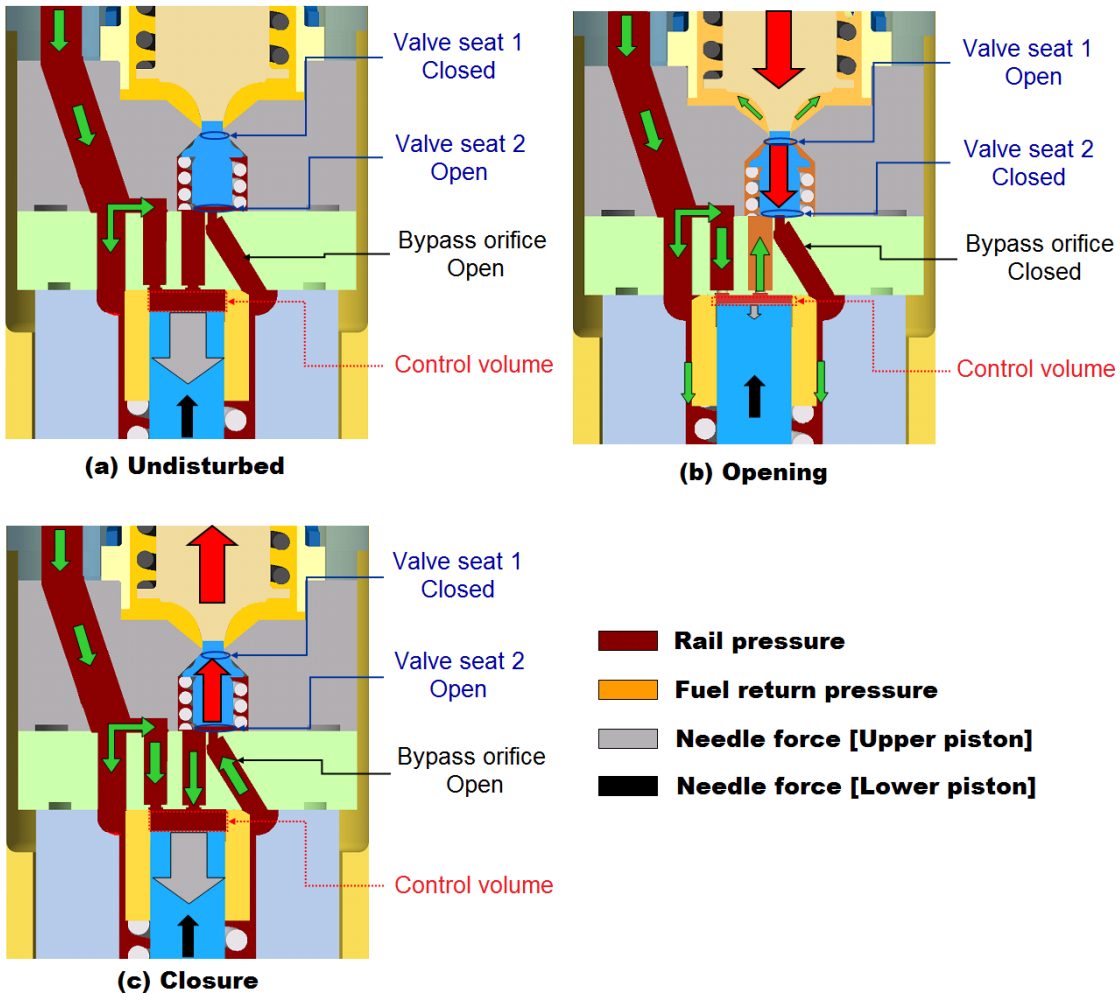

Figure 3. Piezoelectric injector working principle.

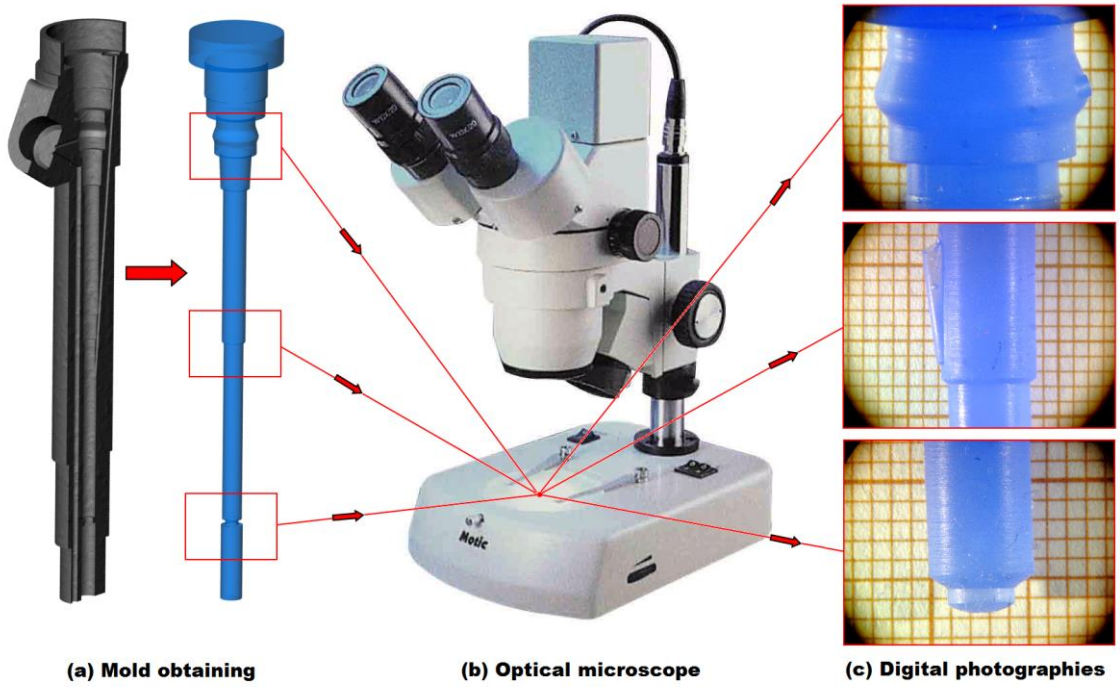

Figure 4. Optical microscope visualization procedure.

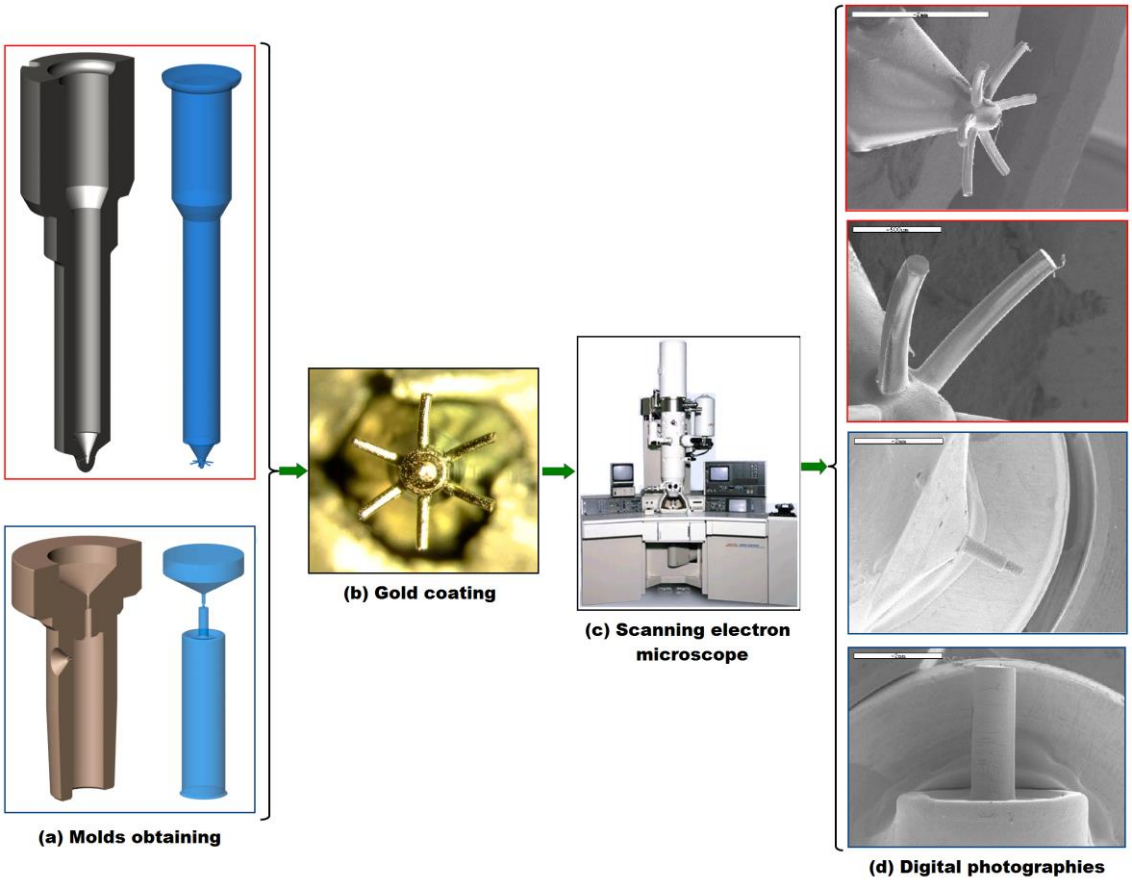

Figure 5. Scanning electron microscope visualization procedure.

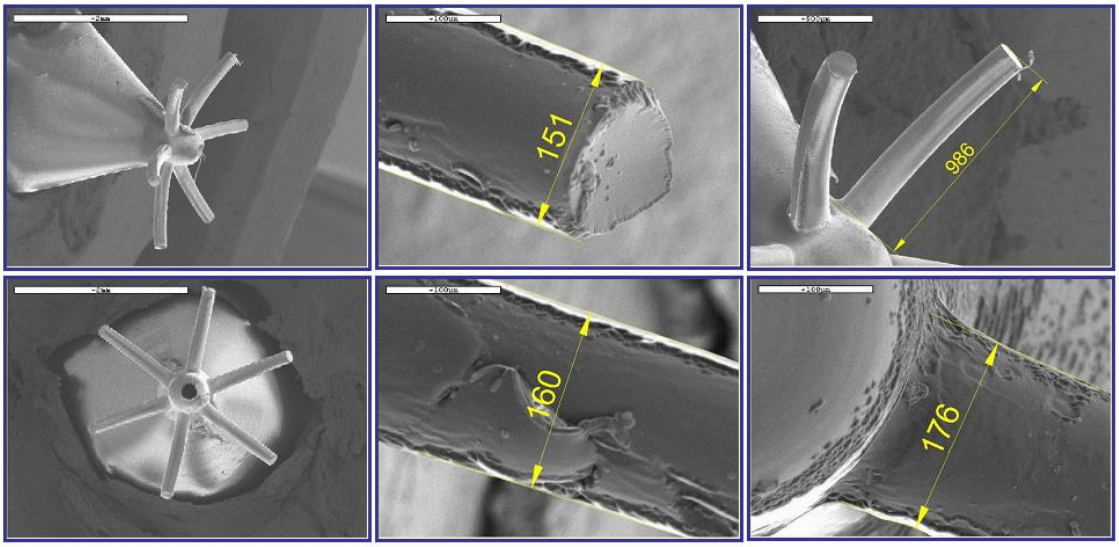

Figure 6. Geometrical characterization of the nozzle orifices.

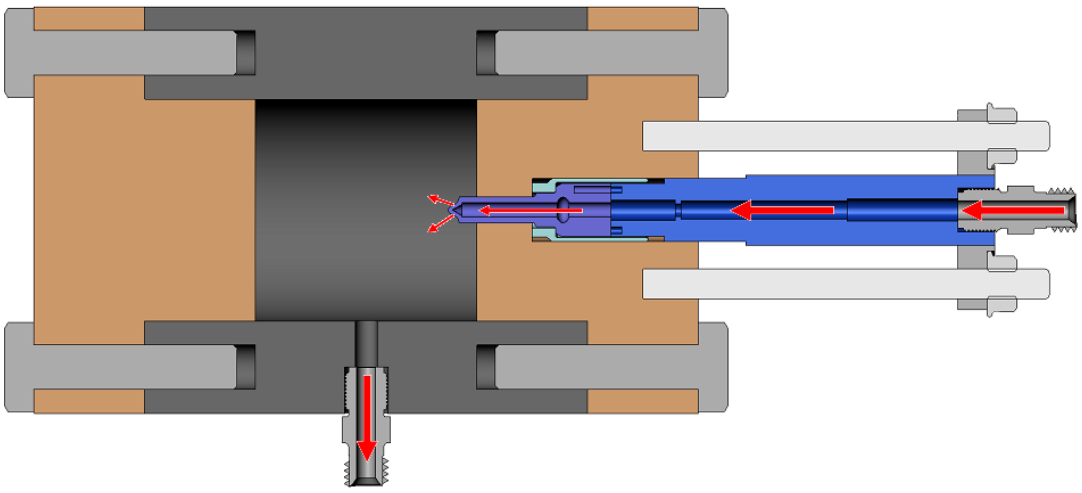

Figure 7. Nozzle orifices hydraulic characterization test rig.

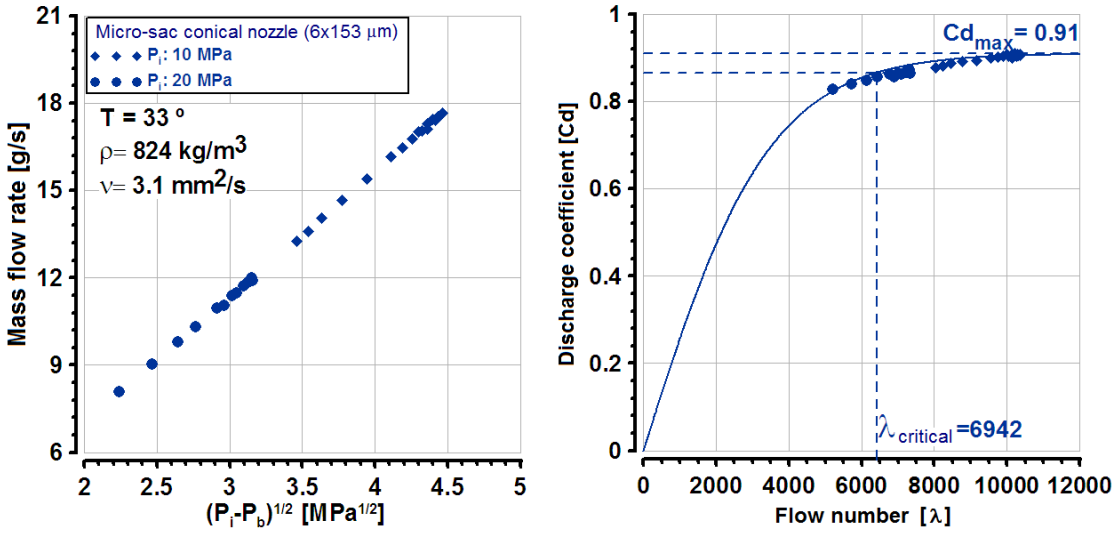

Figure 8. Nozzle hydraulic characterization results.

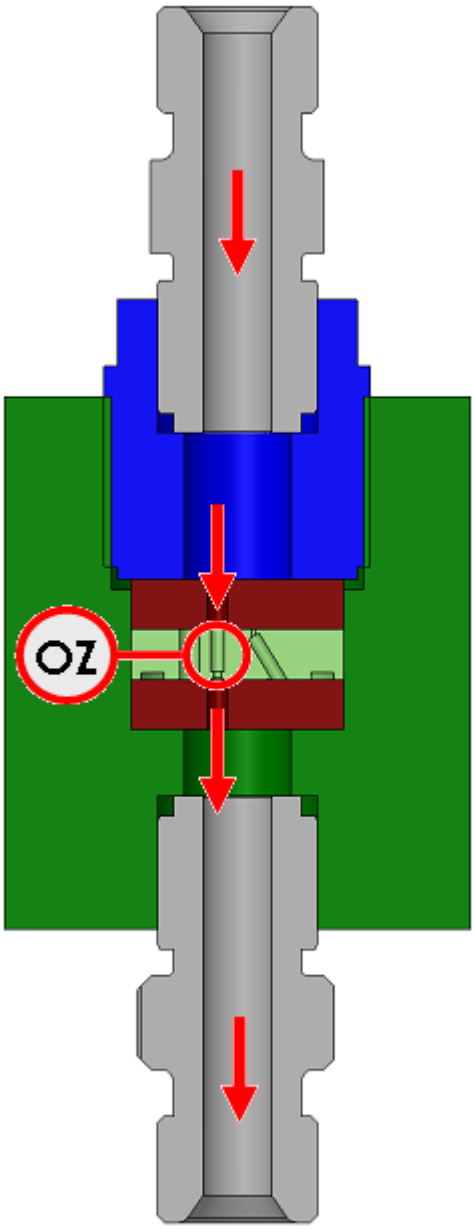

Figure 9. OZ orifice hydraulic characterization test rig.

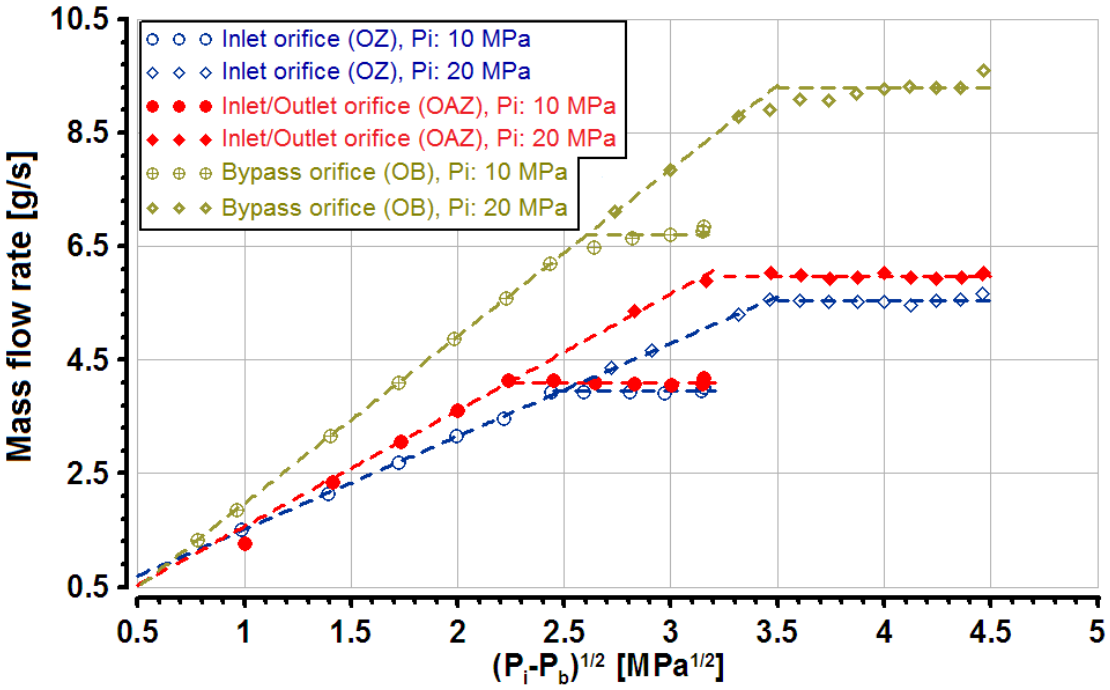

Figure 10. Control orifices hydraulic characterization results.

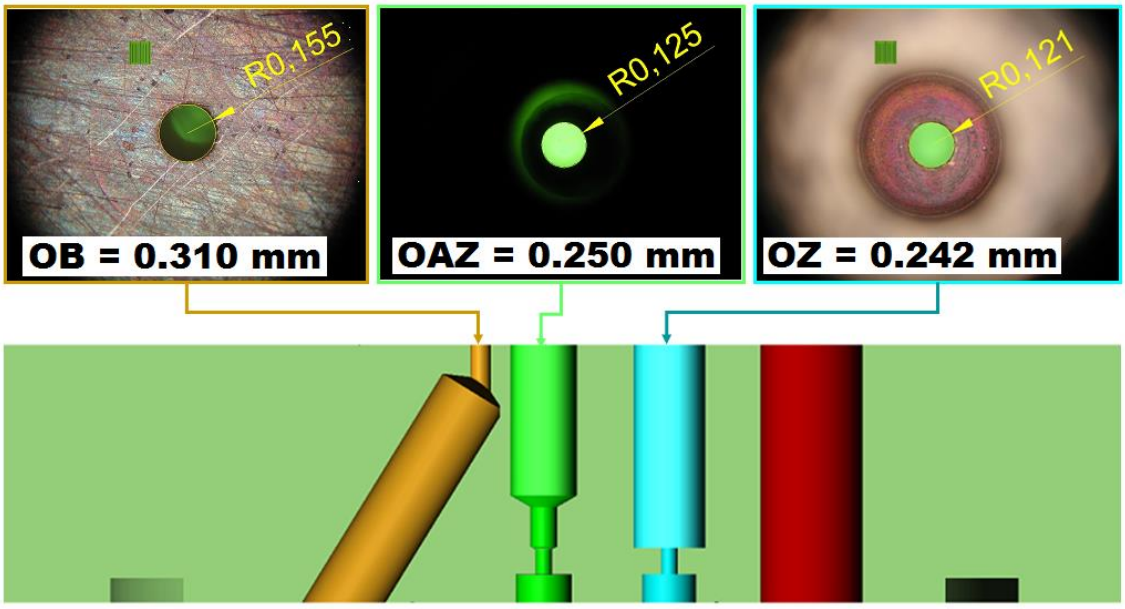

Figure 11. Control orifices geometrical characterization results.

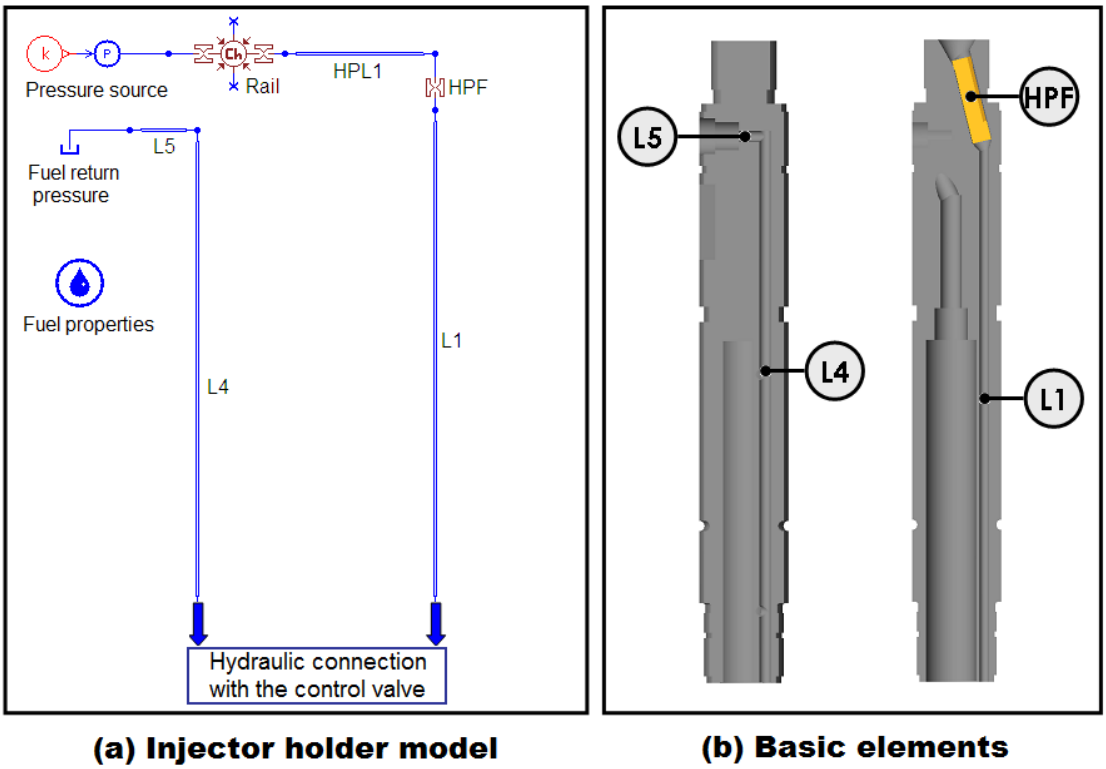

Figure 12. Model and basic elements of the injector holder.

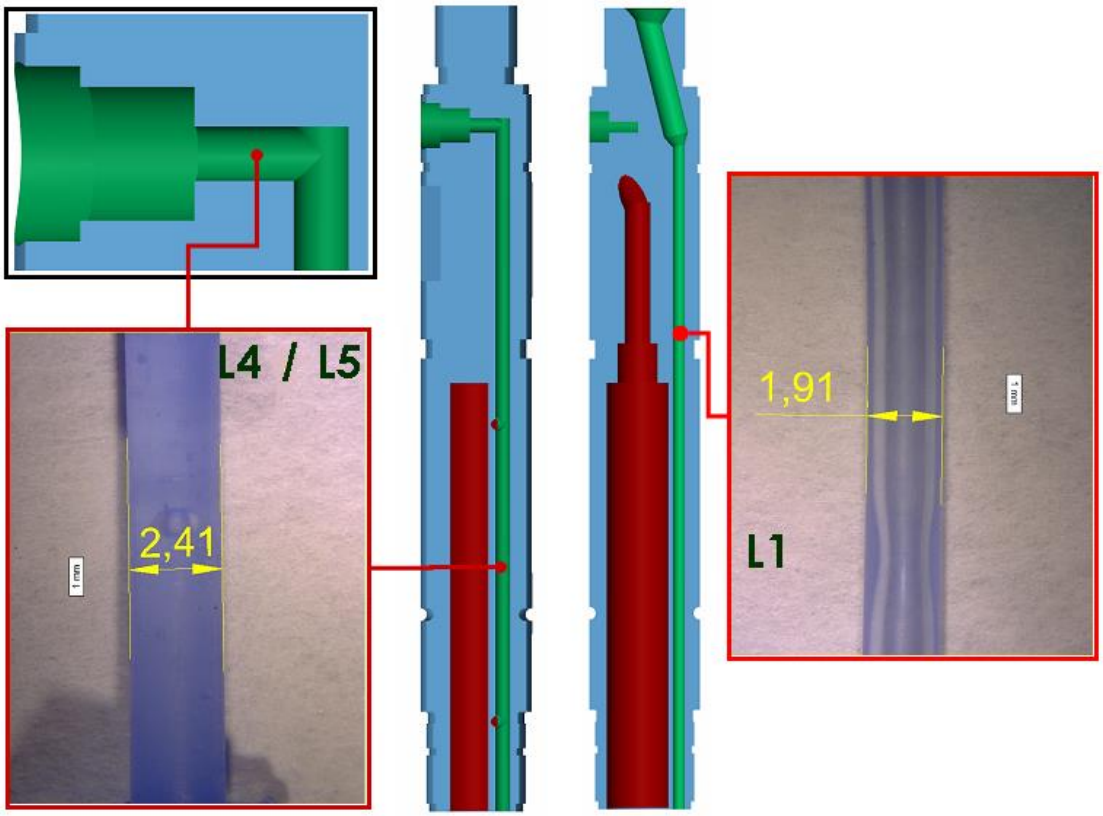

Figure 13. Injector holder lines geometrical characterization.

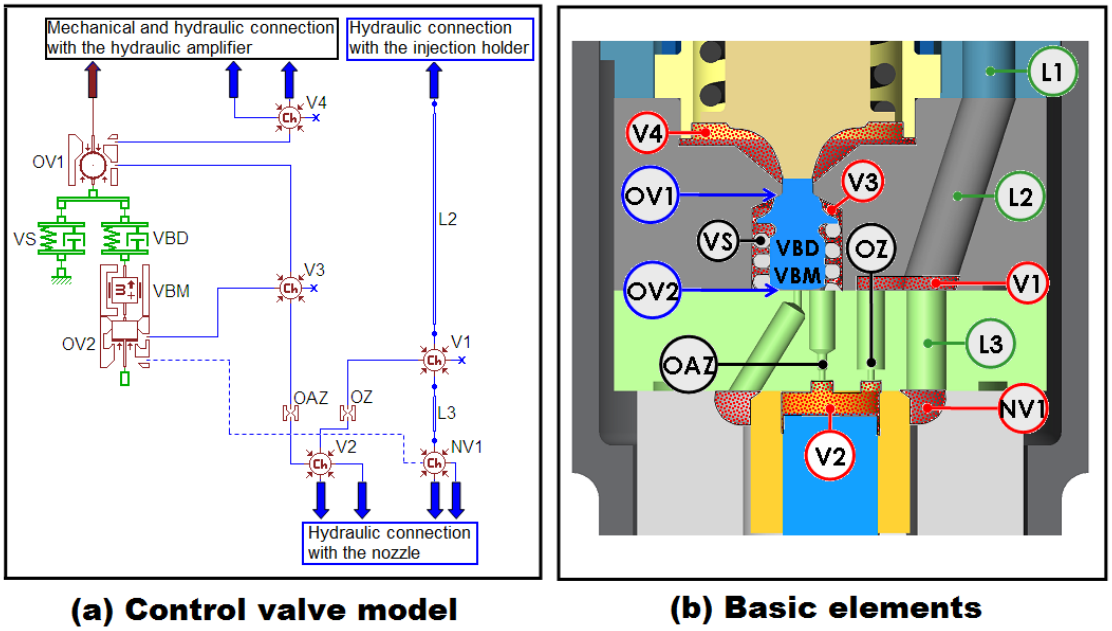

(a) Control valve model **(b) Basic elements**

Figure 14. Model and basic elements of the control valve.

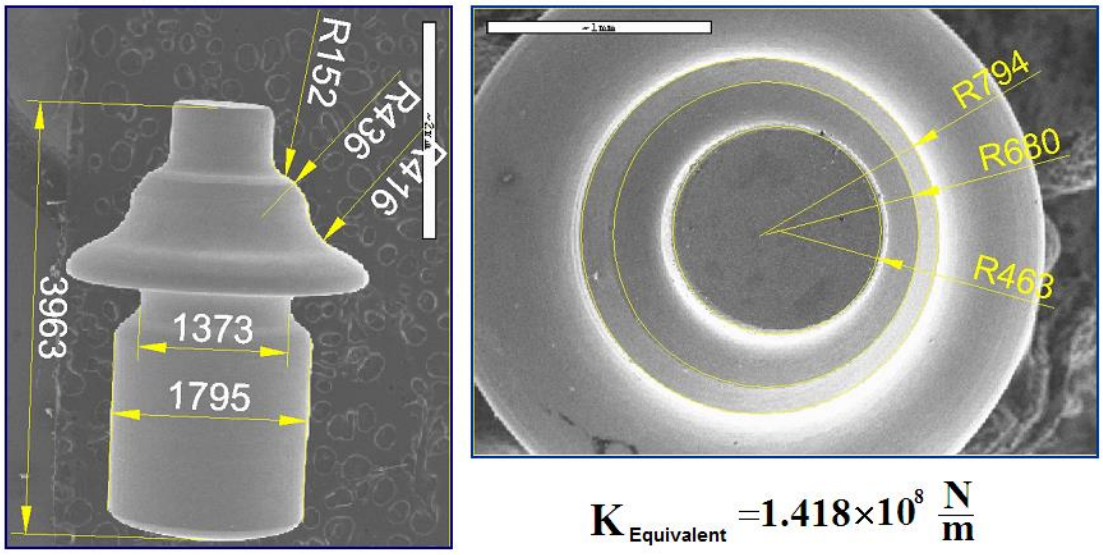

$$K_{Equivalent} = 1.418 \times 10^{8} \frac{N}{m}$$

Figure 15. Valve bolt characterization.

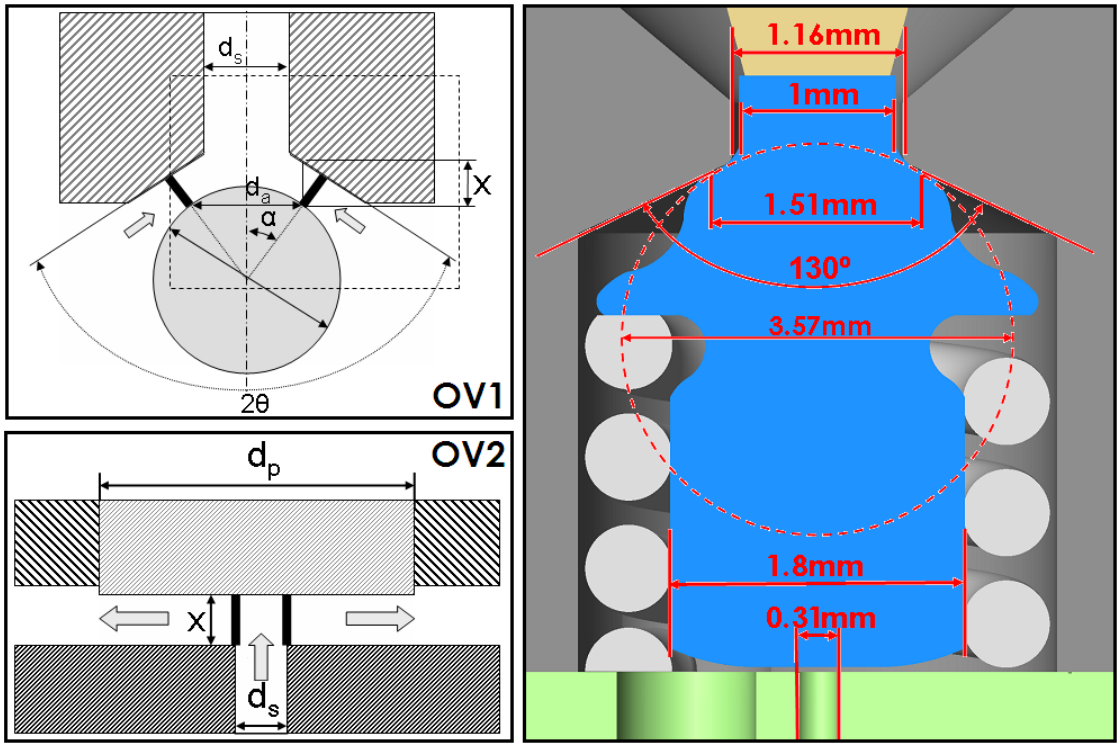

Figure 16. Scheme of the upper and lower control valve seats.

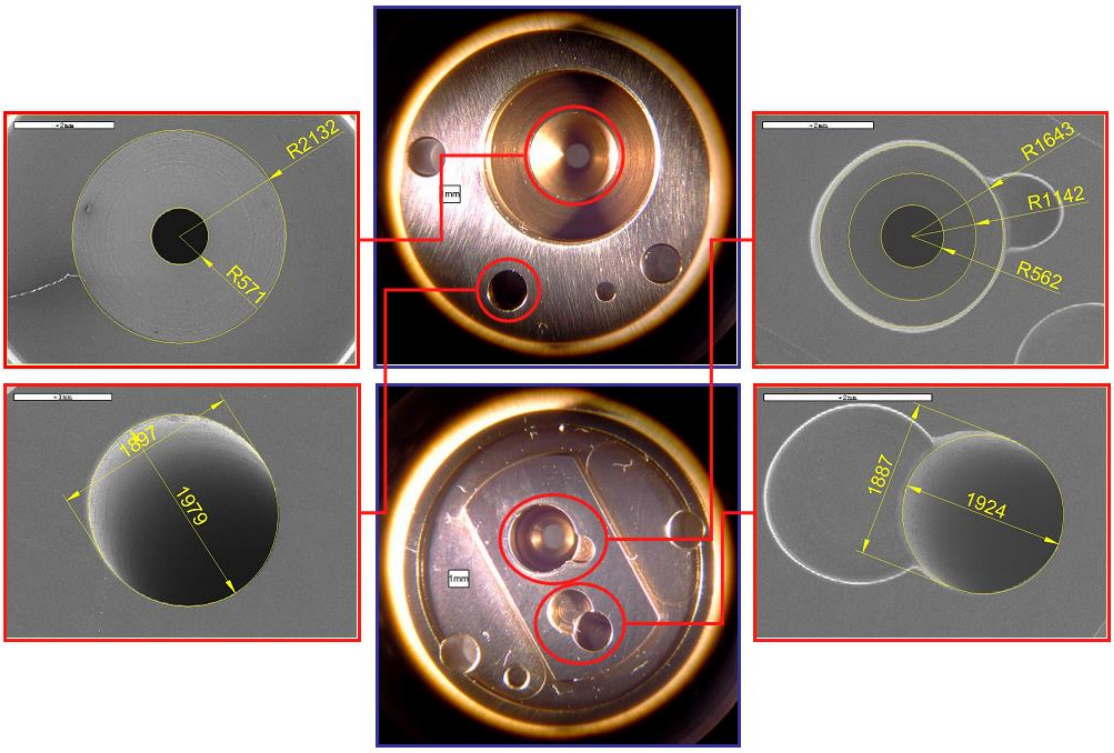

Figure 17. Control valve orifices dimensional characterization.

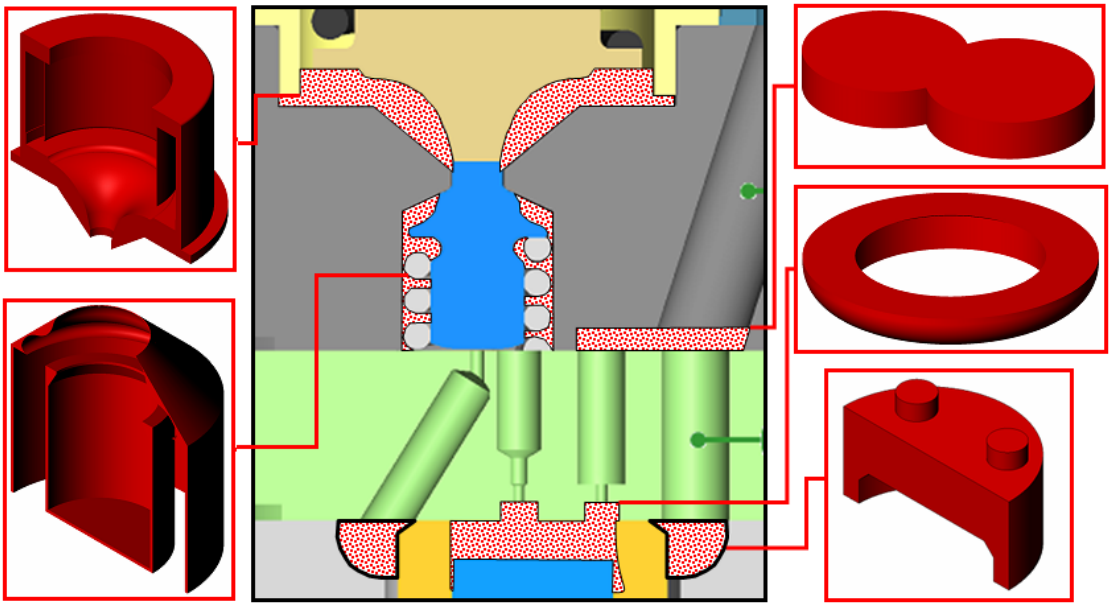

Figure 18. Scheme of the control valve related volumes.

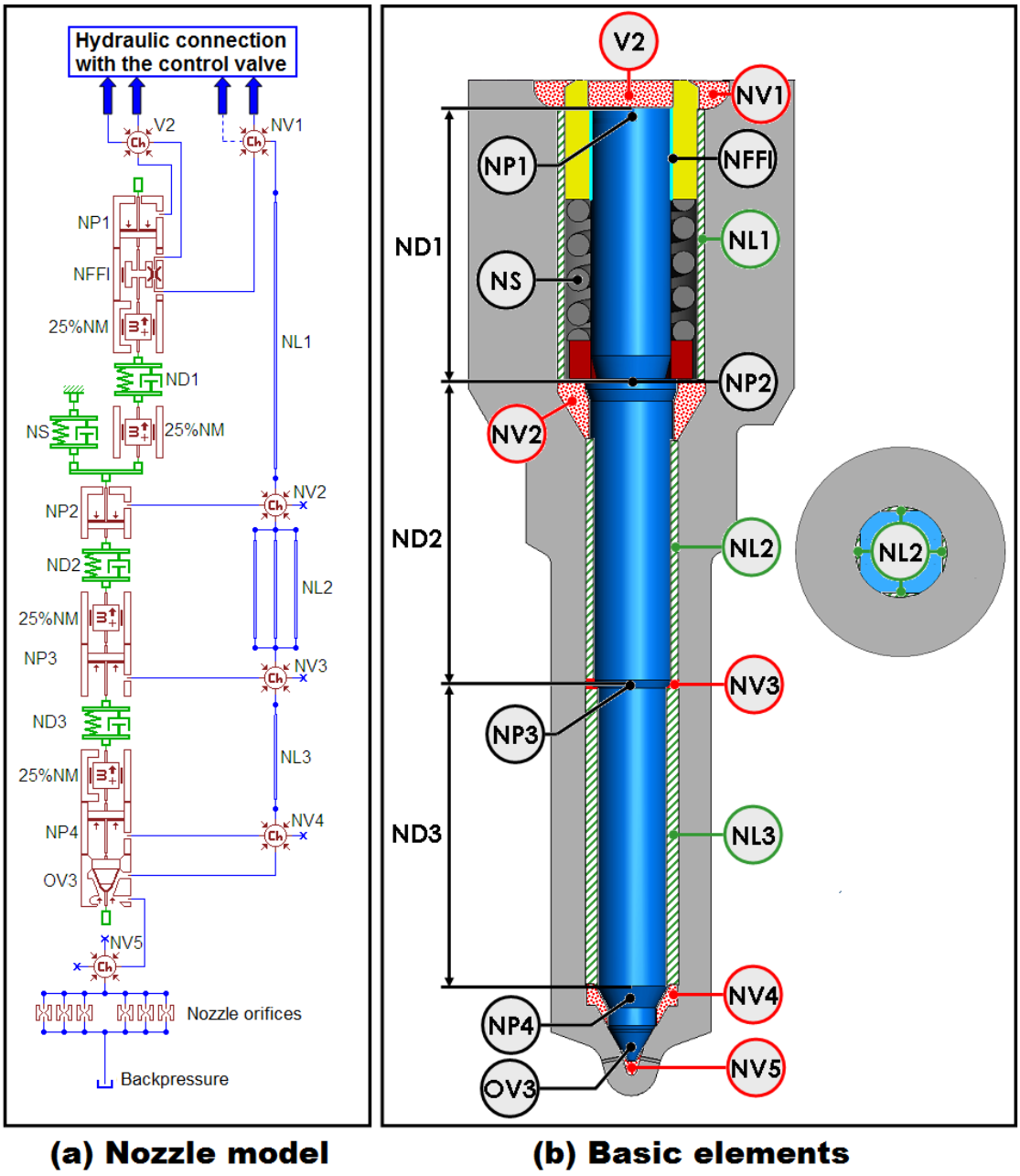

Figure 19. Model and basic elements of the nozzle.

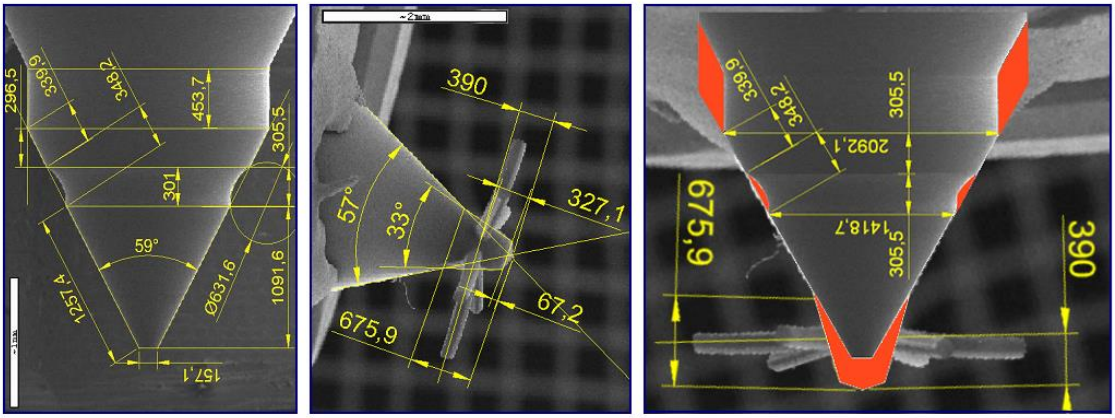

(a) Needle **(b) Nozzle mold** **(c) Overlapping**

Figure 20. Nozzle seat geometrical characterization.

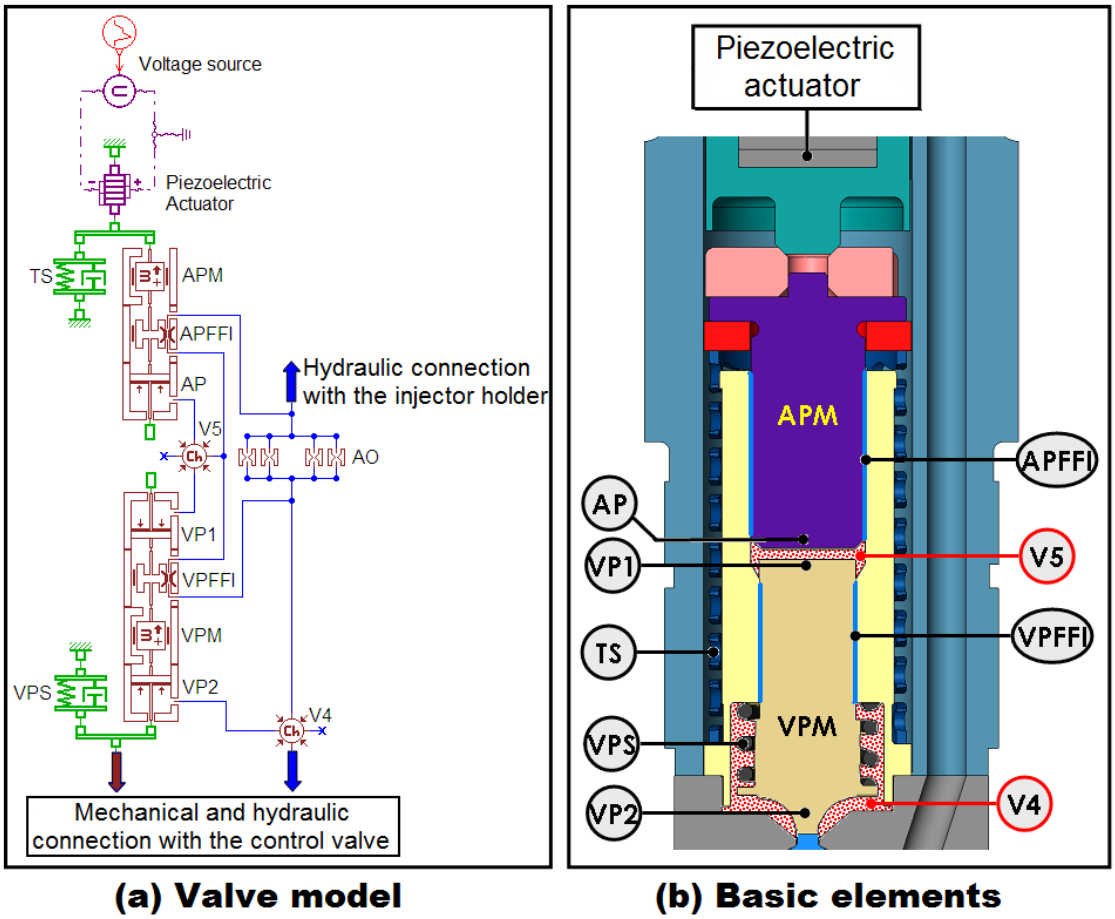

Figure 21. Model and basic elements of the piezoelectric valve.

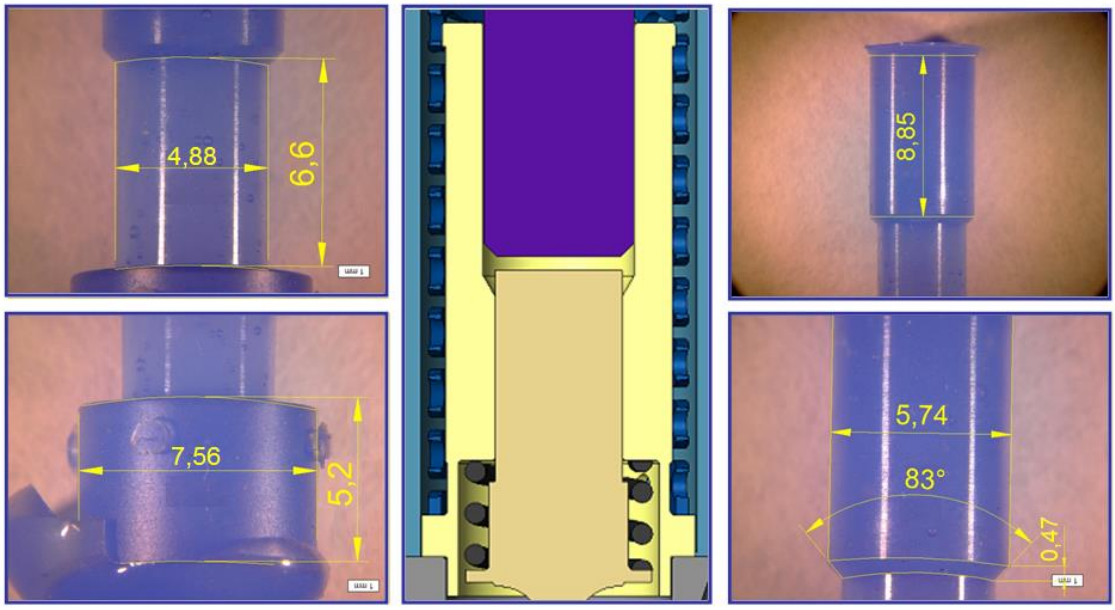

Figure 22. Hydraulic amplifier body geometrical characterization.

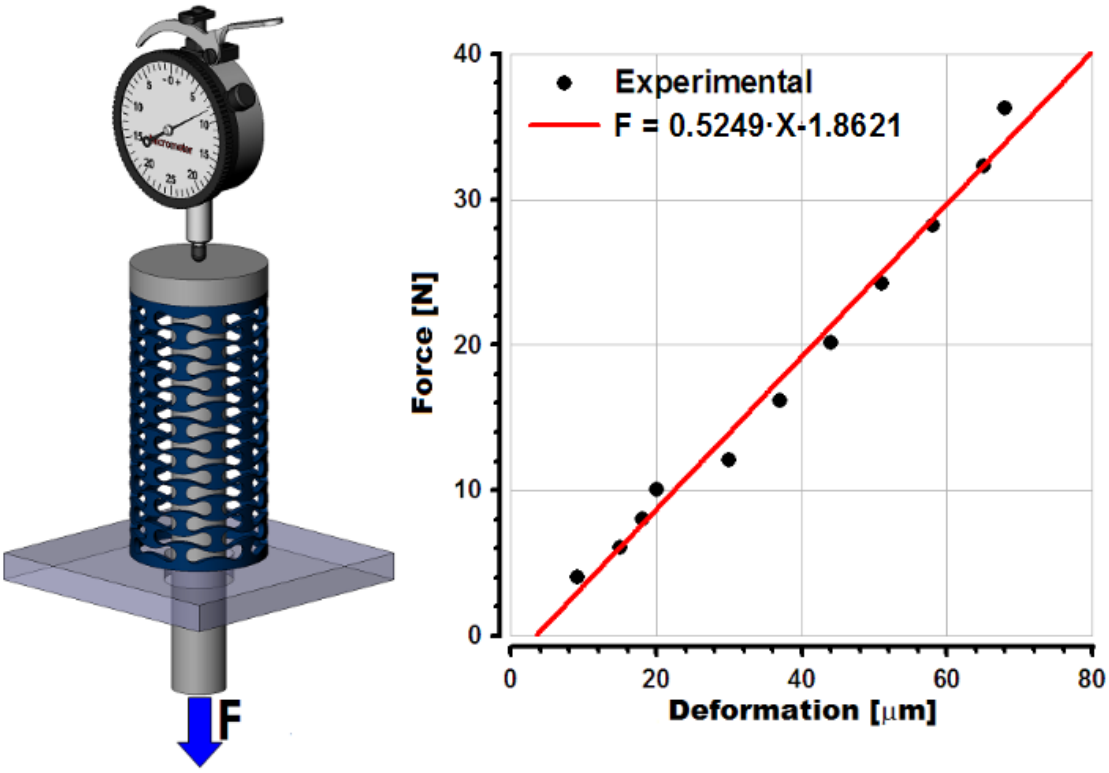

Figure 23. Tube spring (TS) stiffness rate determination.

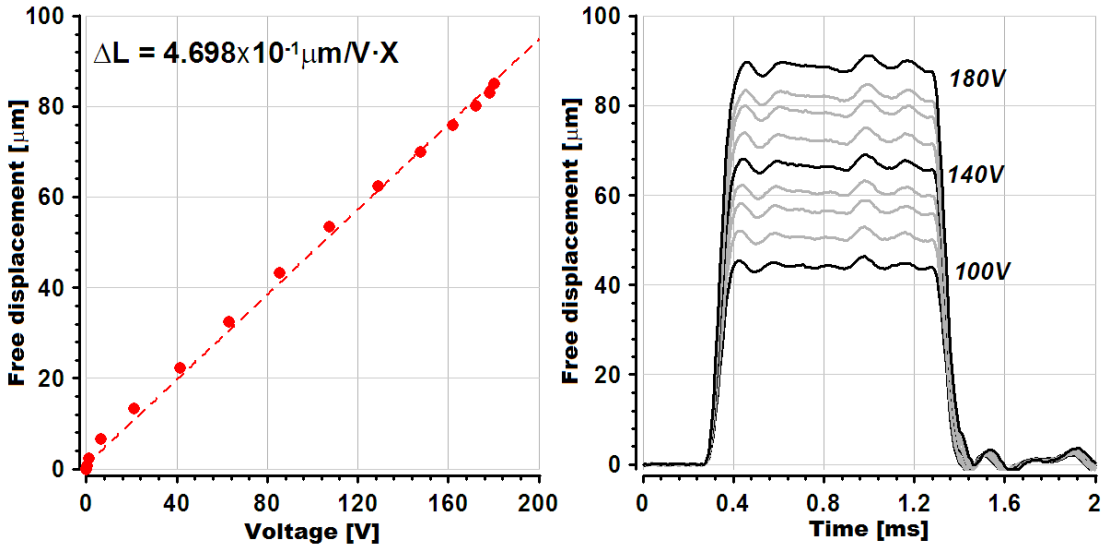

Figure 24. Piezoelectric actuator characterization test.

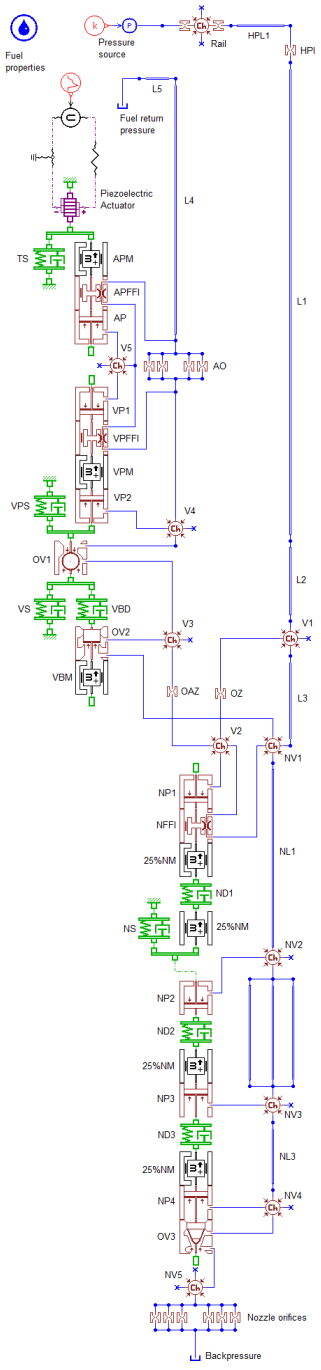

Figure 25. Complete sketch of the injector model including the different parts described.

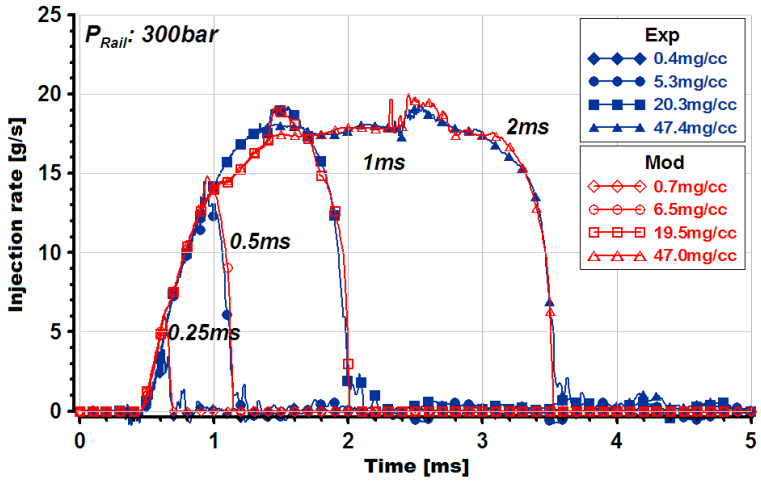
P_{Rail}: 300bar
Exp
0.4mg/cc
5.3mg/cc
20.3mg/cc
47.4mg/cc
Mod
0.7mg/cc
6.5mg/cc
19.5mg/cc
47.0mg/cc
0.25ms
0.5ms
1ms
2ms
Injection rate [g/s]
Time [ms]

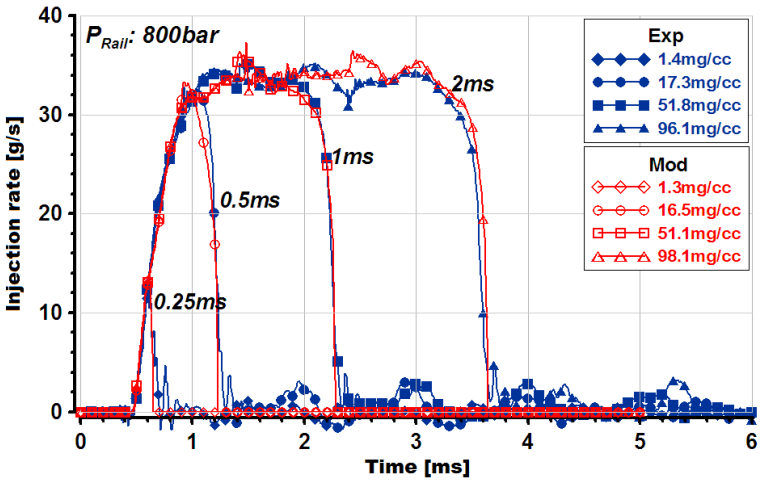
P_{Rail}: 800bar
Exp
1.4mg/cc
17.3mg/cc
51.8mg/cc
96.1mg/cc
Mod
1.3mg/cc
16.5mg/cc
51.1mg/cc
98.1mg/cc
0.25ms
0.5ms
1ms
2ms
Injection rate [g/s]
Time [ms]

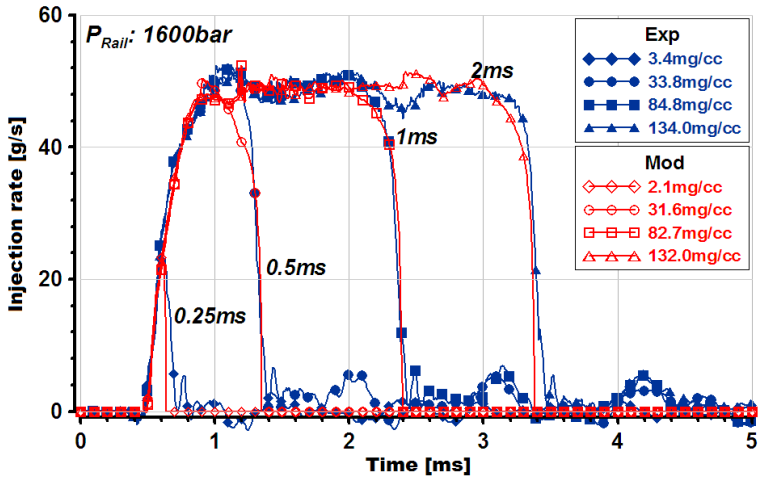
P_{Rail}: 1600bar
Exp
3.4mg/cc
33.8mg/cc
84.8mg/cc
134.0mg/cc
Mod
2.1mg/cc
31.6mg/cc
82.7mg/cc
132.0mg/cc
0.25ms
0.5ms
1ms
2ms
Injection rate [g/s]
Time [ms]

Figure 26. Model validation at different injection pressures and energizing times.

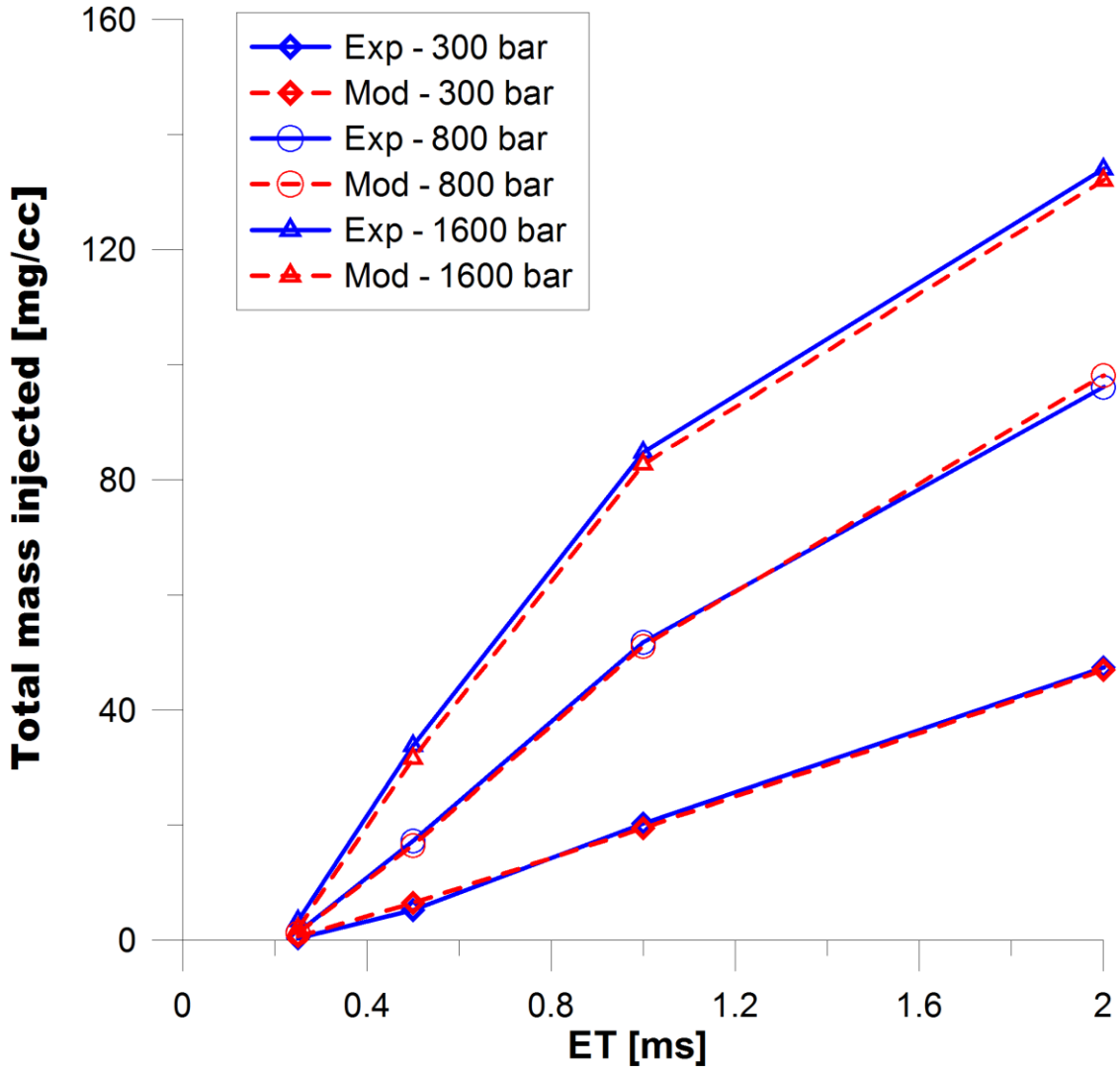

Figure 27. Model validation in terms of total mass injected.

Table 1. Repsol CEC RF-06-99 fuel properties.

Test	Unit	Result	Uncertainty
Density at 15ºC	kg/m^3	843	±0.2
Viscosity at 40ºC	mm^2/s	2.847	±0.42
Volatility			
65% distillated at	ºC	294.5	±3.7
85% distillated at	ºC	329.2	±3.7
95% distillated at	ºC	357	±3.7
Average fuel molecular composition		$C_{13}H_{28}$	

Table 2. Critical parameters of the control orifices.

Orifice	Diameter (µm)	C_{dmax}	$\lambda_{critical}$	$CN_{critical}$	C_c
OZ	0.242	0.86	4000	1.49	0.66
OAZ	0.25	0.94	6150	1.05	0.67
OB	0.31	0.87	9900	1.55	0.68

Table 3. Injector holder model parameters.

Element	Length (mm)	Diameter (mm)	Volume (cm^3)
Rail	-	-	24
HPL1	90	2.5	-
HPF	-	2	-
L1	112.58	1.91	-
L4	116.69	2.41	-
L5	4.345	2.41	-

Table 4. Control valve model parameters.

Element	Length (mm)	Diameter (mm)	Volume (cm^3)	Mass (g)
V4	-	-	0.093709	-
OV1	-	1.16	-	-
V3	-	-	0.00292	-
OV2	-	0.31	-	-
VBM	-	-	-	0.111
OAZ	-	0.25	-	-
V2	-	-	0.02	-
OZ	-	0.242	-	-
V1	-	-	0.0029125	-
L2	7.41	2	-	-
L3	3.69	0.8	-	-
NV1	-	-	0.031423	-

Element	Spring Rate (N/m)	Damper Rating (N/(m/s))
VBD	$2.588 \cdot 10^8$	50
VS	24118	5

Table 5. Nozzle model parameters.

Element	Length (mm)	Diameter (mm)	Volume (cm^3)	Mass (g)
V2	-	-	0.02	-
NP1	-	3.5	-	-
NFFI	3.3	3.501	-	-
NM	-	-	-	4.124
NV1	-	-	0.031423	-
NL1	11.81	2.573	-	-
NV2	-	-	0.032537	-
NP2	-	3.5	-	-
NL2	11.81	0.978566	-	-
NV3	-	-	0.0001	-
NP3	-	3.2	-	-
NL3	13	2.4	-	-
NV4	-	-	0.007281	-
NP4	-	2.14	-	-
OV3	-	0.8	-	-
NV5	-	-	0.000261482	-
Orifices	-	0.151	-	-

Element	Spring Rate (N/m)	Damper Rating (N/(m/s))
ND1	$1.656 \cdot 10^8$	50
NS	$2.952 \cdot 10^4$	5
ND2	$1.592 \cdot 10^9$	50
ND3	$1.039 \cdot 10^8$	50

Table 6. Piezoelectric valve model parameters.

Element	Length (mm)	Diameter (mm)	Volume (cm^3)	Mass (g)
APM	-	-	-	5.896
APFFI	9.7	5.801	-	-
AP	-	5.8	-	-
V5	-	-	0.0106	-
AO	-	1	-	-
VP1	-	4.9	-	-
VPFFI	6.32	4.901	-	-
VPM	-	-	-	2.136
VP2	-	4.8	-	-
V4	-	-	0.093709	-

Element	Spring Rate (N/m)	Damper Rating (N/(m/s))
TS	524867	50
VPS	3833	5